Electrochemical Analysis and Inhibition Assay of Immune-Modulating Enzyme, Indoleamine 2,3-Dioxygenase

Yasuhiro Mie *, Chitose Mikami, Yoshiaki Yasutake, Yuki Shigemura, Taku Yamashita, Hirofumi Tsujino

Posted Date: 3 February 2025

doi: 10.20944/preprints202502.0100.v1

Keywords: immunosuppressive enzyme; inhibition screening; electrochemical assay; redox control; nanoporous electrode

 doi:10.20944/preprints202502.0100.v1

Article

Electrochemical Analysis and Inhibition Assay of Immune-Modulating Enzyme, Indoleamine 2,3-Dioxygenase

Yasuhiro Mie [1,*], Chitose Mikami [1], Yoshiaki Yasutake [1,2], Yuki Shigemura [3], Taku Yamashita [4] and Hirofumi Tsujino [3,5]

[1] Bioproduction Research Institute, National Institute of Advanced Industrial Science and Technology (AIST), Sapporo 062-8517, Japan
[2] Computational Bio Big-Data Open Innovation Laboratory (CBBD-OIL), AIST, Tokyo 169-8555, Japan
[3] Graduate School of Pharmaceutical Sciences, Osaka University, Osaka 565-0871, Japan
[4] School of Pharmacy and Pharmaceutical Sciences, Mukogawa Women's University, Hyogo 663-8179, Japan
[5] Museum Links, Osaka University, Osaka 560-0043, Japan
* Correspondence: yasuhiro.mie@aist.go.jp; Tel.: +81 50 3522 8983

Abstract: An accurate and rapid analysis of human indoleamine 2,3-dioxygenase (hIDO) is crucial for the development of anticancer pharmaceuticals because of the role of hIDO in promoting tumoral immune escape. However, the conventional assay of hIDO is limited by interference from reductants, which are used to reduce the heme iron to begin the hIDO catalytic reaction. Herein, we report a direct electrochemical method to control the redox state of the heme iron and the electrochemical investigation of hIDO. Although the conventional gold electrode did not offer a visible signal for the electron transfer between the electrode and hIDO, the anodized nanostructured gold electrode exhibited a clear nonturnover electrochemical response in an Ar atmosphere. In the presence of oxygen, the bioelectrocatalytic current for the reduction of oxygen, which competes with the oxidation of tryptophan upon the addition of the substrate, was observed, confirming an electrochemically driven hIDO reaction. A well-known inhibitor of hIDO, epacadostat, hindered this catalytic signal according to its concentration, demonstrating the rapid evaluation of its inhibition activity for the hIDO reaction. Through an in silico study using the proposed electrochemical assay system, we discovered a strong inhibitor candidate with a half-maximal inhibitory concentration of 10 nM, similar to that of epacadostat. This suggests the usefulness of the proposed system in drug discovery for hIDO and kynureine pathway-targeted immunotherapy.

Keywords: immunosuppressive enzyme; inhibition screening; electrochemical assay; redox control; nanoporous electrode

1. Introduction

The extremely complex process of clearing foreign and aberrant cells while preventing autoimmunity is performed to maintain multicellular life. This finely tuned balance is frequently mediated by enzymes involved in central metabolism [1]. One such enzyme is human indoleamine 2,3-dioxygenase 1 (hIDO1). It catalyzes the oxidative cleavage of L-tryptophan (Trp) to *N*-formylkynurenine (NFK) by opening the five-membered ring of Trp using molecular oxygen (O_2) [2–4]. Most of Trp is metabolized through the kynurenine (KYN) pathway, and hIDO1 acts as the first and rate-limiting step of the pathway. Thus, this enzyme plays an important role in controlling the relative TRP flux. The overactivation of hIDO1 leads to the upregulation of the KYN pathway, contributing to anxiety, psychosis, cognitive decline, and neurodegenerative disorders [5–8]. It has

 doi:10.20944/preprints202502.0100.v1

been recently discovered that cells that express hIDO1 activity can profoundly alter their environment to suppress the immune response by depleting Trp (the key nutrient required for T-cell activation) and by promoting the production of immunosuppressive kynurenine metabolites [9,10]. Consequently, hIDO1 has attracted attention as an important therapeutic drug target [11]. In addition, a second isoform of hIDO, hIDO2, was discovered and observed to be dysregulated in cancer cells [12], where it may play a crucial role in suppressing antitumor immunity similar to hIDO1.

Considering that hIDO functions as an immunosuppressor, the strong inhibition of the enzyme is expected to deteriorate cancer-cell growth through antitumor immunity. Thus, inhibitor screening is essential for drug discovery. To promote this, the accurate and rapid analysis of hIDO is important. hIDO contains heme iron as the active site, which should be reduced to initiate the Trp oxidation reaction. To date, ascorbate and methylene blue (MB) are commonly used to determine hIDO activity, where ascorbate reduces the MB, which functions as an electron mediator to reduce the heme iron [13–15]. However, the system presents certain challenges. Sono et al. indicated that such a reducing system reduced ferric hIDO by only 25–40% under certain conditions [16]. Such an incomplete reduction of hIDO is supported by resonance Raman spectroscopy [17] and attributed to the relatively low redox potential of the hIDO heme iron. Furthermore, the MB reduced by ascorbate was reoxidized by dioxygen (a substrate for the Trp oxidation reaction by hIDO) [18]. This suggested a difficulty in controlling the oxygen concentration during the assay [16]. For hIDO2, Yuasa et al. reported that the ascorbate and MB system significantly affected the enzymatic reaction [19]. They demonstrated that ascorbate is a weak competitive inhibitor and that MB inhibits hIDO2 at low Trp concentrations while enhancing the activity at higher Trp concentrations. Owing to such phenomena, a more simple and useful assay system for hIDOs is urgently required to develop immunotherapeutic drugs.

The electrochemical method is a useful technique for controlling the electron transfer reaction (oxidation/reduction state) of redox molecules, using an electrode as an electron donor or acceptor by applying the electrochemical potential. The direct electron transfer between the electrode and redox enzyme active site (e.g., heme iron in IDO) is often difficult because the active site is generally located in polypeptide chains. Thus, the enzyme molecule at the electrode surface must be properly oriented to minimize the distance of electron transfer since the rate of electron transfer exponentially decreases with an increase in distance [20–22]. Recently, conductive nanomaterials, such as nanocarbons and metal nanoparticles, have been frequently used to modify the surface of electrode substrates. Furthermore, the given nanostructured surface is effective for achieving direct electron transfer with the enzyme active site [23–25]. In addition, the nanostructurization of the electrode materials is also useful. Nanoporous gold (NPG) prepared via the anodization of a planar gold surface is a prospective material. This is because of its advantages of high conductivity, chemical inertness, physical stability, reusability, high catalytic activity, and facile surface modification [26,27]. In addition, the anodization strategy for producing NPG is extremely simple, facile, and rapid. We recently developed a strategy for controlling the NPG surface structure [28] and immobilized heme redox enzymes, such as cytochrome P450, neuroglobin, and cytoglobin, on the structure-controlled NPG. Thereafter, we observed that the NPG structure strongly enhanced the electron transfer reaction with the electrode and heme iron of these enzymes [29–31]. To the best of our knowledge, there have been no reports on the electrochemical analysis of hIDO with direct electron transfer at an electrode.

Here, we examined the redox state control of hIDO1 using an NPG electrode with direct electron transfer and demonstrated the electrochemical analysis of hIDO1 without interference from chemical reductants. An efficient electrochemical inhibitor assay system was constructed, and a strong inhibitor candidate was discovered using the system.

 doi:10.20944/preprints202502.0100.v1

2. Results and Discussion

2.1. Electrochemical Redox Control of hIDO1 Using the NPG Electrode with Direct Electron Transfer

The direct electron transfer reaction between the enzyme active site and the electrode surface provides a simple system for the electrochemical investigation of the enzyme. Thus, we investigated the electrode surface structure to achieve the direct electron transfer. The voltammetric responses of hIDO1 immobilized the planar gold and NPG electrodes obtained in a phosphate buffer solution (pH = 7.5) containing 0.1 M NaCl at a potential scan rate of 0.2 V s^{-1} (Figure 1). Figures 1A and B show the morphology of the surfaces of the NPG and planar electrodes, respectively, with a nanostructure comprising pores and ligaments on the NPG surface. The immobilization was conducted at the hydroxy-terminated thiol-modified gold surface through covalent bonding with the hydroxy group of the hIDO1 surface. As shown, a clear couple of reductive and oxidative currents were observed at the NPG electrode of hIDO1 (Figure 1C), indicating the rapid direct electron transfer between the heme iron of hIDO1 and electrode surface. The redox potential ($E^{0\prime}$) obtained from the voltammogram was –145 mV at pH 7.5. This value was comparable to that (–68 mV) obtained at a pH of 7.0 measured using the dye(s) titration method [32], considering the difference in the measured method and pH condition for one electron transfer reaction ($Fe^{3+} + e^- = Fe^{2+}$). The charges of the oxidative and reductive current signals corresponded to 1.0 ± 0.25 nmol cm^{-2}, indicating the monolayer coverage of hIDO1. The intensity of the faradaic (oxidative and reductive) currents from hIDO1 practically remained unchanged within the tested period of up to 24 h. The results showed the electrochemical control of the redox states of the heme iron in hIDO1. Conversely, the planar gold electrode did not exhibit a faradaic current signal, suggesting the usability of the proposed NPG electrode to electrochemically investigate hIDO1. When hIDO1 was immobilized on the electrode through an amino group on its surface, less response was observed at the NPG electrode, probably due to the conformational changes in the enzyme (not shown). Thus, we used the hIDO1-immobilized NPG electrode through hydroxy group covalent bonding. The direct electron transfer could have resulted from the curvature effect of the nanoporous structure [22].

The cyclic voltammograms of hIDO1 were analyzed to understand its electrochemical properties. Figure 2 shows the potential scan rate dependence of the voltammetric behavior. The oxidative and reductive peak currents exhibited a linear relationship with the scan rate (Figure 2a), indicating that the electrochemical responses originated from the surface-bound hIDO1. The peak separation between the anodic and cathodic peak potentials increased with the potential scan rate. This provided an apparent heterogeneous electron transfer rate constant (k_s') of 21 s^{-1} from the fitting of a trumpet plot (peak position vs. scan rate, Figure 2b), using a simulation program developed by Jeuken et al. [34]. The value of the constant was comparable to that of neuroglobin, which exhibited similar heme iron coordination structures during the redox reaction, immobilized at the NPG electrode (46 s^{-1}) [30]. We additionally investigated the mutated hIDO1, R231Q, whose activity for Trp cleavage was considerably low (described below). The mutant showed a couple of redox peak currents (Figure 3) similar to that of the wild type (WT), indicating the rapid electron transfer to the electrode surface. Although the redox potential was slightly (20 mV) more negative, the k_s' of the R231Q mutant estimated from the trumpet plot was 17 s^{-1}, which was close to that of the WT. This indicated that this mutation gave no significant influence on the electron transfer kinetics and the structural changes that occurred during the redox reaction of hIDO1 for both WT and R231Q were similar.

 doi:10.20944/preprints202502.0100.v1

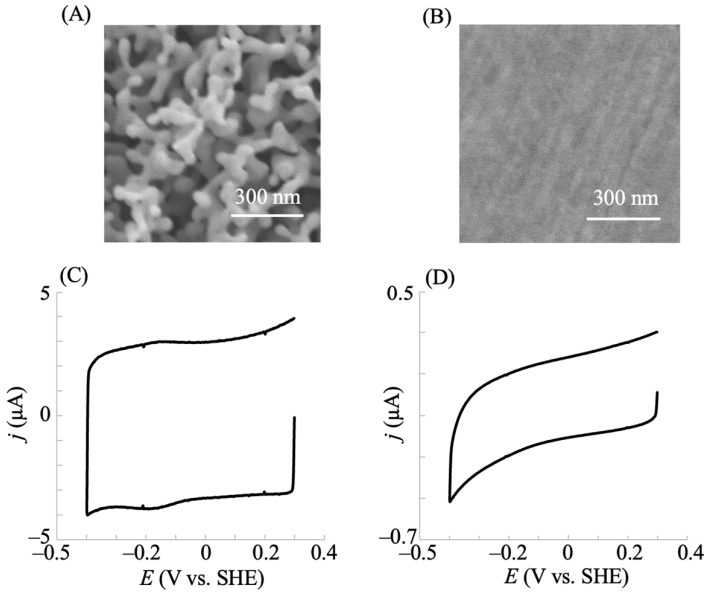

Figure 1. SEM images of the NPG (A) and planar gold (B) electrodes within the range of 1 × 1 μm, and cyclic voltammograms of IDO1 immobilized on the NPG (C) and planar gold (D) electrodes in a 0.1 M phosphate buffer solution containing 0.1 M NaCl at a scan rate of 0.2 V s^{-1}.

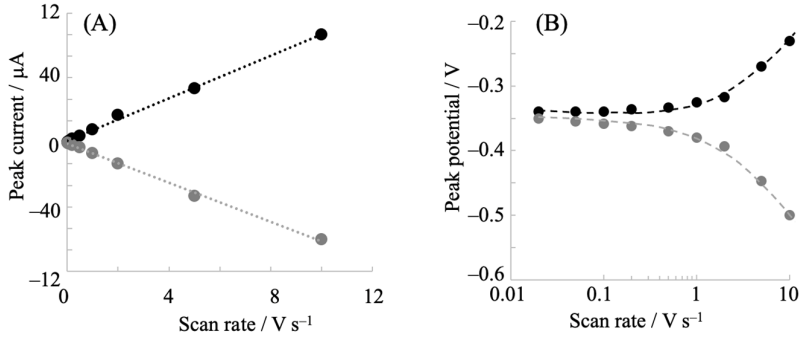

Figure 2. Relationship between (A) the oxidative (black circle) and reductive (gray circle) peak currents and (B) the oxidative (black circle) and reductive (gray circle) peak potentials against potential scan rates for the hIDO1-immobilized NPG electrode. Voltammetry was conducted in a 0.1 M phosphate buffer solution (pH 7.5) containing 0.1 M NaCl under Ar atmosphere.

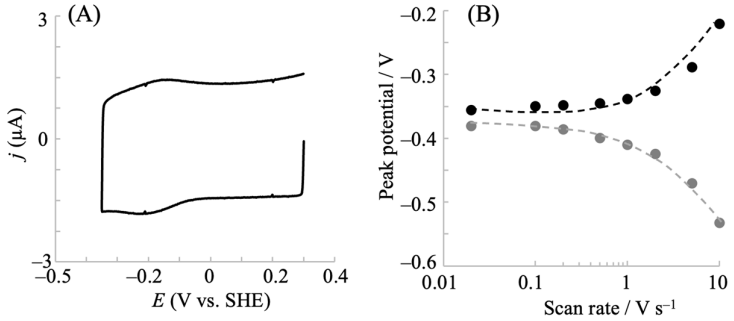

Figure 3. (A) Cyclic voltammogram of hIDO1 R231Q mutant immobilized on an NPG electrode in a 0.1 M phosphate buffer solution containing 0.1 M NaCl at a scan rate of 0.2 V s^{-1}. (B) The corresponding trumpet (peak potential vs. potential scan rate) plot for R231Q.

 doi:10.20944/preprints202502.0100.v1

2.2. Electrocatalytic Reductive Reaction with hIDO in the Presence of Molecular Oxygen and Trp

Considering that the electrochemical redox control of hIDO1 was successfully achieved using NPG, its electrocatalytic reaction was investigated in the presence of substrates. First, we investigated the reaction in the presence of molecular oxygen (O_2, one of the substrate of hIDO1). As shown in Figure 4A, the electrocatalytic reductive current was observed in the presence of O_2, which appeared at the redox potential in the non-turnover voltammogram of hIDO1 in the absence of O_2 (red line in Figure 4A) at a scan rate of 20 mV s^{-1}. The catalytic current increased with an increase in the concentration of dissolved O_2. Furthermore, the ratio of the reductive currents in the presence of O_2 compared with that in the absence of O_2 increased with a decrease in the potential scan rate. The control experiments with NPG electrodes modified with 6-hydroxy-1-hexanethiol (HHT), and HHT coupled with bovine serum albumin did not result in such catalytic currents (Figure 4B). The results showed that the reduced hIDO1 reacted with molecular oxygen. This kind of bioelectrocatalytic response with oxygen has been reported for an electrode immobilized with myoglobin, which has His residue coordinated to the heme iron at the distal site similar to hIDO1. The reaction was recognized as the electrochemical catalytic reduction of O_2 to produce hydrogen peroxide [34–36]. The oxidation reaction of the ferrous heme iron by the produced hydrogen peroxide to ferric iron was suggested from the voltammograms [37]. hIDO1 has a heme iron coordination structure similar to that of myoglobin, and a relatively. Thus, we expect that the bioelectrocatalytic reaction for molecular oxygen occurred at the hIDO1-immobilized NPG electrode similar to the myoglobin case as follows:

$$\text{hIDO1}(Fe^{3+}) + \quad e^- \rightleftharpoons \text{hIDO1}(Fe^{2+}) \tag{1}$$

$$\text{hIDO1}(Fe^{2+}) + O_2 \rightarrow \text{hIDO1}(Fe^{2+})\text{–}O_2 \tag{2}$$

$$\text{hIDO1}(Fe^{2+})\text{–}O_2 + 2H^+ + 2e^- \rightarrow \text{hIDO1}(Fe^{2+}) + H_2O_2 \tag{3}$$

$$2\text{hIDO1}(Fe^{2+}) + H_2O_2 + 2H^+ \rightarrow 2\text{hIDO1}(Fe^{3+}) + 2H_2O \tag{4}$$

The electrochemically reduced hIDO1 (Eq. (1)) was bound to oxygen to become an oxy-form (Eq. (2)), and it was converted into the deoxy-form with the production of hydrogen peroxide at the electrode (Eq. (3)). Thereafter, the deoxy-form was oxidized to the ferric form by the hydrogen peroxide (Eq. (4)).

Next, electrocatalysis using the hIDO1-immobilized electrode in the presence of Trp and oxygen was investigated. Prior to the addition of Trp to the system, voltammetry was conducted in the presence of 35–45 μM oxygen, and the aforementioned hIDO1-based oxygen reductive catalysis was confirmed. This range of oxygen concentrations was selected because they are physiologically relevant levels [38]. The addition of Trp lowered the electrocatalytic oxygen reduction current according to its concentration (Figure 5a). The electrochemically reduced hIDO1 (hIDO1(Fe^{2+})) was first bound to oxygen to become the oxy-form (hIDO1(Fe^{2+})–O_2) (Eqs. 1 and 2). Thereafter, Trp was bound to the distal heme pocket of hIDO1(Fe^{2+})–O_2 to produce a ternary complex, hIDO1(Fe^{2+})–O_2–Trp (Eq. (5)).

$$\text{hIDO1}(Fe^{2+})\text{–}O_2 + \text{Trp} \rightarrow \quad \text{hIDO1}(Fe^{2+})\text{–}O_2\text{–Trp} \tag{5}$$

$$\text{hIDO1}(Fe^{2+})\text{–}O_2\text{–Trp} \rightarrow \text{IDO1}(Fe^{2+}) + \text{KYN} \tag{6}$$

The ternary complex converted Trp into NFK. The k_{cat} range for the NFK formation by hIDO1 within an oxygen concentration range of 30–50 μM was reported to be 7.1–8.5 s^{-1} [38]. Thus, upon the addition of Trp, we expected the reaction of Eq. (3) in the electrocatalytic oxygen reduction by hIDO1 to be hindered by the consumption of hIDO1(Fe^{2+})–O_2 species by the inherent Trp cleavage reaction of hIDO1 (Eqs. (5) and (6)). Therefore, the decrease in the bioelectrocatalytic oxygen reductive signal upon the addition of Trp (Figure 5a) would be reasonable, indicating that this decrease can be a measure of the hIDO1 Trp cleavage catalysis.

 doi:10.20944/preprints202502.0100.v1

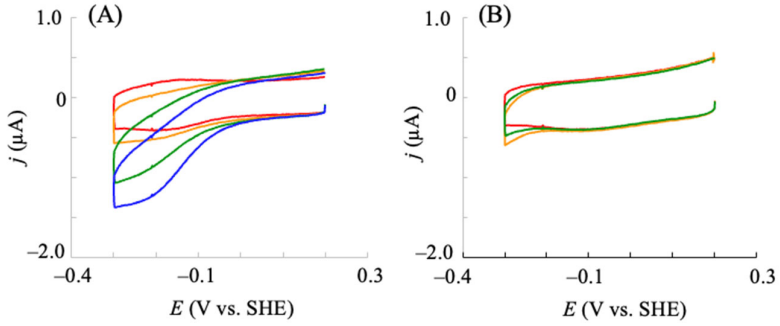

Figure 4. Cyclic voltammograms of NPG electrodes modified with hIDO1 (A) and bovine serum albumin (B) in a phosphate buffer (pH = 7.5) containing 100 mM NaCl upon the addition of molecular oxygen at 20 mV s^{-1}. [O_2]: 0 (red line), 11 (orange line), 20 (green line), 38 (blue line) μM in (A), and 0 (red line), 35 (orange line), 48 (green line) μM in (B). .

To further confirm the electrochemical assay of Trp catalysis by hIDO1, we conducted measurements with R231Q-mutated hIDO1, which exhibited a lower catalytic activity for Trp conversion compared with that of the WT. The k_{cat}/Km of R231Q was smaller by three orders of magnitude than that of the WT. As shown in Figure 5B (red line), the R231Q mutant exhibited electrocatalytic reductive current in the presence of oxygen and the absence of Trp, similar to that of the WT, suggesting that the aforementioned oxygen reduction reaction occurred. However, no significant change was observed with the addition of Trp (Figure 5B), different from that of the WT case (Figure 5A). R231Q had considerably less binding of Trp by the mutation at the position, which connects to the Trp, while the oxygen can be bound to its heme iron. Thus, the above electrochemical observation for WT and R231Q was consistent with these facts. The Trp concentration that reduces the half of the current decrease for WT was estimated to be 7 μM (Figure 5C). This was slightly smaller than the reported K_M obtained via the conventional method for converting Trp into NFK (18–25 μM) [38,39]. The addition of MB in the conventional strategy has been reported to decrease the affinity of human IDO1 for Trp [40]. Therefore, the value obtained through the present method could be reasonable because MB was absent in the electrochemical system. The results showed that the hIDO1 activity can be electrochemically evaluated using the present NPG electrode without the conventional reducing agents that affect hIDO reactions.

 doi:10.20944/preprints202502.0100.v1

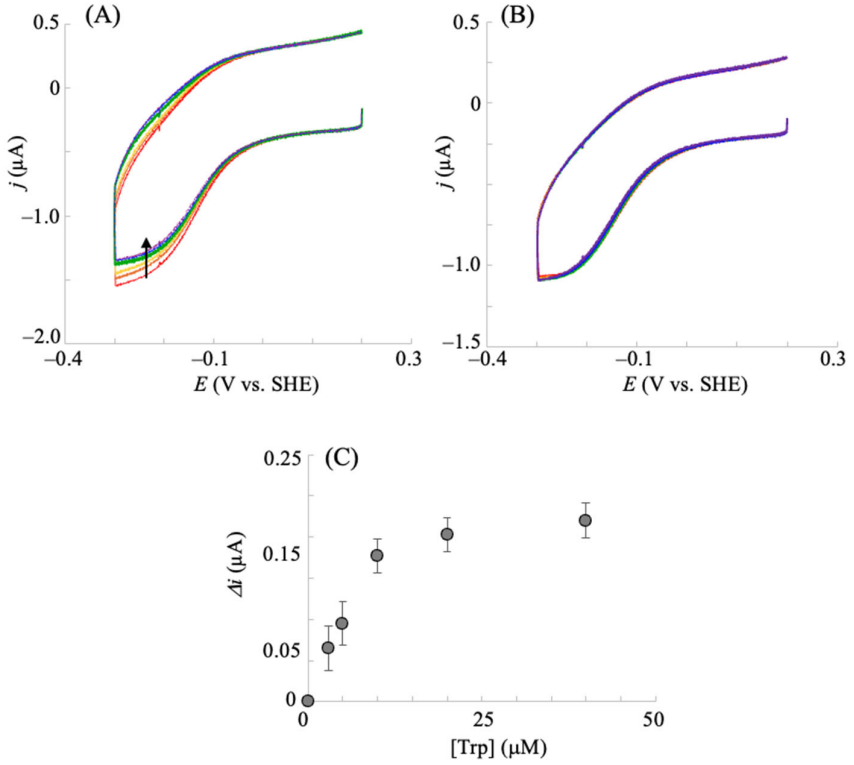

Figure 5. Cyclic voltammograms of hIDO1 WT (A) and R231Q (B) immobilized NPG electrodes upon the addition of Trp in a phosphate buffer (pH = 7.5) containing 100 mM NaCl and ca. 40 μM molecular oxygen. The Trp concentration was increased from 0 to 40 μM (red → orange → yellow → green → blue → purple). The corresponding plot for [Trp] vs. the decreased current (C). Values are presented as the mean ± SD (n = 3 independent experiments).

2.3. Electrochemical hIDO Inhibition Assay

The inhibition of hIDO1 for converting Trp into NFK is important for developing anticancer therapeutics. As described above, the electrochemically driven hIDO1 reaction was achieved, and the rapid analysis of the inhibition reaction is expected by the electrochemical strategy. Thus, we investigated whether the change in the electrochemical response of hIDO1 was observed after the addition of the inhibitor(s). First, the well-known hIDO1 inhibitor, epacadostat (Figure 6A), was examined. Upon the addition of epacadostat, the stable electrocatalytic response of hIDO1 in the presence of O_2 and Trp decreased (Figure 6B). The degree of the decrease increased with an increase in the concentration of the inhibitor added to the electrochemical system and practically plateaued above a certain concentration. T The apparent half-maximal inhibitory concentration (IC_{50}) was estimated to be 15 nM from the plot of the inhibitor concentration vs. the degree of decrease in the catalytic current (Figure 6C). This electrochemically calculated value was comparable to reported values (7–15 nM) obtained via cell-based assays [41]. A biochemical assay for isolated/purified hIDO1 using ascorbate and MB provided IC_{50} values above those obtained via cell-based assays [41,42]. The authors claim that the phenomenon results from the complexity of the ascorbate and MB system. Therefore, the results showed that the present electrochemical system with the hIDO1-immobilized NPG electrode is suitable for the inhibition screening of the immune-modulating enzyme without the influence of the aforementioned additives.

Next, we investigated whether the present electrochemical inhibition assay could be used to identify new IDO inhibitors. Ten compounds with top hits by in silico screening were purchased and examined via electrochemical hIDO1 analysis in the presence of O_2 (40 μM) and Trp (500 μM). Most of the tested compounds did not affect the electrochemical responses when added to the system. One

 doi:10.20944/preprints202502.0100.v1

compound, whose chemical structure is shown in Figure 7A, selected by the multiple target screening (MTS) method (MTS-7), considerably decreased the electrochemical reductive signal (Figure 7B), indicating the inhibition of the hIDO1 catalytic reaction of Trp metabolism. The plot of the candidate concentration and the decrease in the reductive current (enzymatic activity) shown in Figure 7C provided an IC_{50} value of approximately 10 nM. This value was comparable with that of epacadostat and indicates the potency of the strong inhibitor for the hIDO1 reaction. Molecular docking simulations were performed to assess the binding compatibility of MTS-7 to the active site pocket of hIDO1. The best docking pose (binding affinity, −8.3 kcal/mol) was compared with the epacadostat model bound to the hIDO1 active site determined via a crystallographic study (PDB code, 5WN8) [2]. The docking pose between hIDO1 and MTS-7 is drawn in Figure 8, superimposed on the bound epacadostat model. As shown, the phenyl group of MTS-7 practically occupied the same location in the active site pocket of hIDO1 as the 3-bromo-4-fluorophenyl moiety of epacadostat. Contrarily, the hydrophobic trimethyl group of MTS-7 lay adjacent to a loop structure comprising amino acid residues 236–241 of IDO1. This position differs from that occupied by the solvent-exposed hydrophilic sulfamoylamino moiety of epacadostat. Overall, MTS-7 appears to be able to fit well and bind to the active site pocket of hIDO1 by isolating the hydrophobic trimethyl group from the solvent.

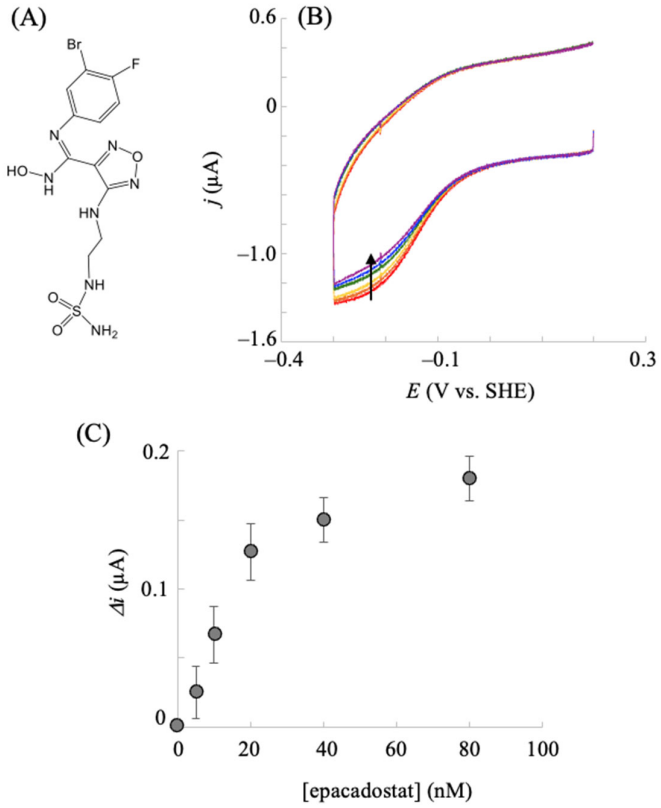

Figure 6. Chemical structure of the epacadostat (A). Voltammetric responses of hIDO1 modified NPG electrode upon the addition of epacadostat in a phosphate buffer (pH = 7.5) containing 100 mM NaCl, 40 μM O_2, and 500 μM Trp at a scan rate of 0.02 V s^{-1} (B). The corresponding plot for [epacadostat] vs. the decreased current (C). Values are presented as the mean ± SD (n = 3 independent experiments).

 doi:10.20944/preprints202502.0100.v1

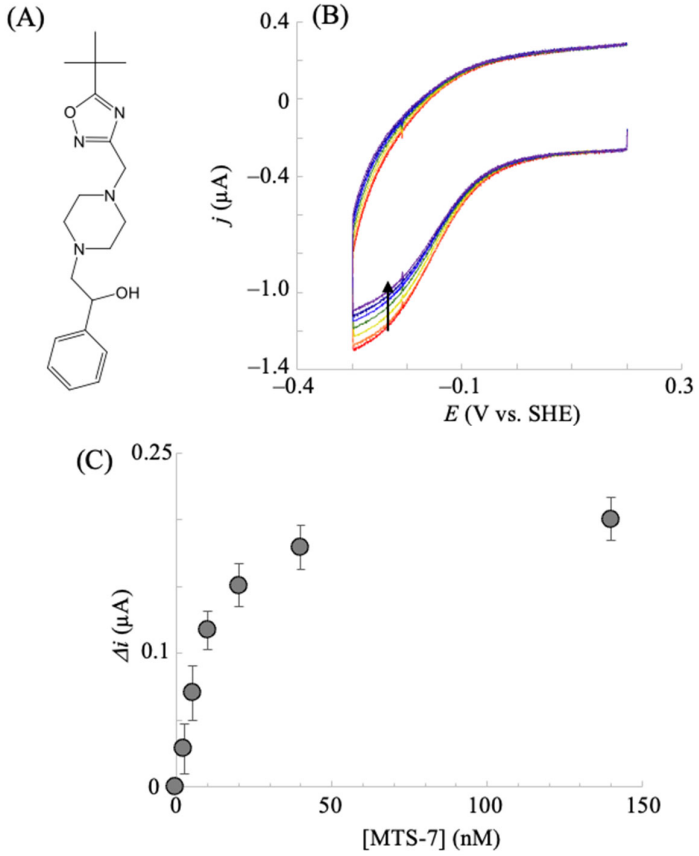

Figure 7. Chemical structure of the predicted candidate (MTS-7) by MTS calculation (A). Voltammetric responses of hIDO1 modified NPG electrode upon the addition of epacadostat in a phosphate buffer (pH = 7.5) containing 100 mM NaCl, 40 μM O_2, and 500 μM Trp at a scan rate of 0.02 V s^{-1} (B). The corresponding plot for [epacadostat] vs. decreased current (C). Values are presented as the mean ± SD (n = 3 independent experiments).

Finally, we performed the conventional hIDO1 inhibition assay for MTS-7 with ascorbate and MB as an electron supply system. Contrary to the result obtained via the aforementioned electrochemical assay, a strong inhibition was not observed (data not shown). We suspect that the considerably higher (three order of magnitudes) concentration of MB inhibited the binding for MTS-7. Although the sulfamoylamino group of epacadostat was exposed to the solvent region, the trimethyl groups of MTS-7 lay alongside the amino acids of 236–241 in the heme pocket, where the hydrophobic MB may be located, to transfer electrons to the heme iron. The proposed method is free from this kind of concern because reductants and/or electron transfer mediators are not required.

Thus, we concluded that the present electrochemical system with the NPG surface is an adequate analytical method for hIDO1 activity without interference from reductants and electron transfer mediators, whose phenomena are observed using the conventional method.

 doi:10.20944/preprints202502.0100.v1

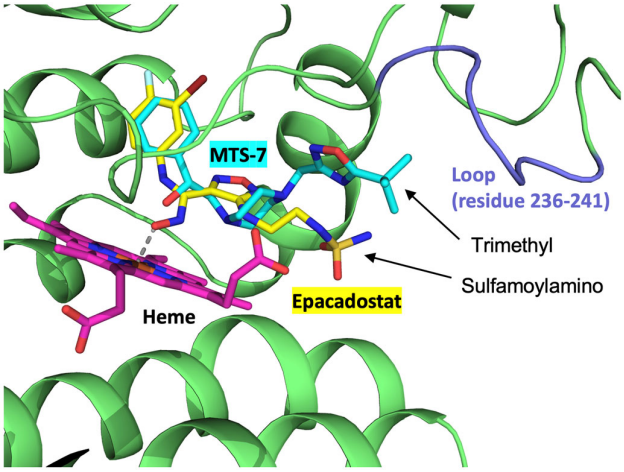

Figure 8. The best docking pose between hIDO1 (PDB code, 5WN8) and MTS-7. The bound epacadostat observed in the structure of 5WN8 is shown. The carbon atoms of MTS-7, epacadostat, and heme are shown in cyan, yellow, and magenta, respectively. The hIDO1 structure is shown in green ribbon representation. The loop region of hIDO1 in the vicinity of the trimethyl of MTS-7 (residues 236–241) is colored light blue.

3. Materials and Methods

3.1. Reagents

6-hydroxy-1-hexanethiol (HHT) for the gold surface modification was purchased from Sigma-Aldrich, and was used as received. Epacadostat and inhibitor candidates were obtained from MedChemexpress Co., Ltd. and Namiki Shoji, Co., Ltd., respectively. All the aqueous solutions were prepared using ultrapure water (18 MΩ cm).

3.2. Preparation of hIDO1 Enzymes

Following a study [43], hIDO1 was expressed in an *Escherichia coli* system, followed by extraction and chromatography to obtain a highly purified enzyme. The gene encoding hIDO1 was ligated into an expression vector (pET3a), and transfected *E. coli* were cultured in a lysogeny broth medium with 0.1 g/L ampicillin (110 rpm, 37°C). When the culture attained an optical density of 0.6 at 600 nm, isopropyl β-(D) thiogalactopyranoside and hemin were successively added to final concentrations of 5 and 7 μM, respectively, to induce protein expression. Culturing was continued at 4,500 g and 4°C for 10 h. Cells were harvested and frozen at −80°C and lysed in a 20 mM potassium phosphate buffer (pH = 6.5). The soluble fraction was isolated by ultracentrifugation (20,000 × *g*), and the supernatant was applied to a hydroxyapatite gel column (BIO-RAD), followed by purification using a CM Sepharose column (GE Healthcare).

3.3. Fabrication of Nanostructured Electrode and hIDO1 Immobilization

A gold disk electrode (Bioanalytical Systems, Ø = 3 mm) was polished using diamond and alumina slurries, and its surface was electrochemically cleaned using 0.5 M H_2SO_4 serving as a conventional (planar) gold electrode [28]. The cleaned planar electrode was put into the solution of 0.5 M HCl solution and an anodized potential about ~1.36 V vs. Ag|AgCl|sat.KCl was applied for ~3 min to fabricate the nanoporous gold (NPG) structure, as has been reported [30]. The surface area of the anodized (nanostructured) gold surface was estimated using a voltammogram recorded at a scan rate of 0.1 V^{-1} in H_2SO_4 [44], and the surface roughness (*R*f) was calculated by dividing the surface area by the geometrical area. Here, an *R*f below 5 was used in the present study to minimize the effect of the mass transfer limitation of the substrates/inhibitor into the deep pore of the NPG [30]. The morphology of the NPG surface was mainly analyzed by scanning electron microscopy (SEM) characterization (S-4300 FE-SEM, Hitachi Ltd., Japan). The electrode surface was modified with thiol

 doi:10.20944/preprints202502.0100.v1

compounds using the 0.5 mM ethanolic solution of each modifier. The hIDO1 molecule was immobilized onto the HHT-coated surface by casting a 0.1 mM hIDO1 solution with 10 mM 1,2-bis (trimethoxysilyl)ethane [45] through a hydroxy group (NPG–O–Ngb).

3.4. Electrochemical Measurements and hIDO1 Assay

Voltammetry was conducted utilizing an electrochemical analyzer (CH Instruments Inc., USA) with a normal three-electrode configuration consisting of an Ag|AgCl|sat.KCl reference electrode, a Pt auxiliary electrode, and a hIDO1 immobilized working electrode. The potentials reported in this work were converted to the standard hydrogen electrode (SHE). Bioelectrocatalytic measurements were performed by controlling the O_2 concentration using a mixed gas controller (Yamato Sangyo, Japan).

3.5. In Silico Study

In silico screening was performed using the program MF myPresto (ver. 3.2, FiatLux, Tokyo, Japan). The multiple target screening (MTS) [46] and docking score index (DSI) [47] methods were applied for the in silico screening against the library consisting of approximately 5,000,000 chemical compounds. An atomic model of the hIDO1 structure for the MTS method was obtained from the Protein Data Bank with accession code 5WN8 [2]. Epocadostat was used as a known active compound (inhibitor) for hIDO1 in the DSI method. Ten commercially available compounds that hit the top rankings (Namiki Shoji Co., Ltd., Tokyo, Japan) were subjected to electrochemical inhibition assays. Molecular docking between hIDO1 and the 2-(4-{[5-(2-methyl-2-propanyl)-1,2,4-oxadiazol-3-yl]methyl}-1-piperazinyl)-1-phenylethanol (MTS-7) was performed using the program AutoDock Vina (ver. 1.1.2) [48]. The configured input files were generated using AutoDock Tools (ver. 1.5.6) [49]. The simulation box for docking calculations that fully cover the catalytic pocket of IDO1 was set up with a dimension of 30 × 28 × 30 Å. Molecular drawings were generated using PyMOL (ver. 2.3.4, Schrödinger LLC, New York, NY, USA).

4. Conclusions

Here, to adequately analyze the hIDO1 activity, an electrochemical strategy was applied. Although the conventional gold electrode failed to reduce hIDO1, the NPG electrode electrochemically enabled the redox state control of the heme iron in hIDO1. The Trp metabolism activity of hIDO1 was monitored based on the decrease in the electrochemical current for the bioelectrocatalytic oxygen reduction reaction through hIDO1. These phenomena were further confirmed via a hIDO1 mutation study. Furthermore, we performed the screening for the hIDO1 inhibitors using the present electrochemical system and successfully discovered a strong inhibitor for hIDO1. The study findings indicate the efficacy of the proposed electroanalytical method.

Author Contributions: Y.M.: Conceptualization, methodology, investigation, data curation, funding acquisition and writing–original draft. C.M.: Investigation, and data curation. Y.Y.: Methodology, investigation, data curation, and writing–review and editing. Y.S.: Investigation, and data curation. T.Y.: Conceptualization, and investigation. H.T.: Methodology, investigation, data curation, and writing– review and editing.

Funding: This work was partly supported by the JSPS KAKENHI Grant Number JP19K07024 and JP24K02171.

Data Availability Statement: Data are available within the article.

Acknowledgments: The authors would like to thank Enago (www.enago.jp) for the English language review.

Conflicts of Interest: The authors declare no conflict of interest.

 doi:10.20944/preprints202502.0100.v1

References

1. Nelp, M. T.; Kates, P. A.; Hunt, J. T.; Newitt, J. A.; Balog, A.; Maley, D.; Zhu, X.; Abell, L.; Allentoff, A.; Borzilleri, R.; Lewis, H. A.; Lin, Z.; Seitz, S. P.; Yan, C.; Groves, J. T., Immune-modulating enzyme indoleamine 2,3-dioxygenase is effectively inhibited by targeting its apo-form. *Proc. Natl. Acad. Sci. U S A* **2018**, 115, (13), 3249-3254.
2. Lewis-Ballester, A.; Pham, K. N.; Batabyal, D.; Karkashon, S.; Bonanno, J. B.; Poulos, T. L.; Yeh, S. R., Structural insights into substrate and inhibitor binding sites in human indoleamine 2,3-dioxygenase 1. *Nat. Commun.* **2017**, 8, (1), 1693.
3. Capece, L.; Lewis-Ballester, A.; Yeh, S. R.; Estrin, D. A.; Marti, M. A., Complete reaction mechanism of indoleamine 2,3-dioxygenase as revealed by QM/MM simulations. *J. Phys. Chem. B* **2012**, 116, (4), 1401-13.
4. Booth, E. S.; Basran, J.; Lee, M.; Handa, S.; Raven, E. L., Substrate Oxidation by Indoleamine 2,3-Dioxygenase: EVIDENCE FOR A COMMON REACTION MECHANISM. *J. Biol. Chem.* **2015**, 290, (52), 30924-30.
5. Oxenkrug, G., Serotonin - Kynurenine Hypothesis of Depression: Historical Overview and Recent Developments. *Curr. Drug Targets* **2013**, 14, (5), 514-521.
6. Miura, H.; Ozaki, N.; Sawada, M.; Isobe, K.; Ohta, T.; Nagatsu, T., A link between stress and depression: Shifts in the balance between the kynurenine and serotonin pathways of tryptophan metabolism and the etiology and pathophysiology of depression. *Stress* **2008**, 11, (3), 198-209.
7. Guillemin, G. J.; Brew, B. J., Implications of the kynurenine pathway and quinolinic acid in Alzheimer's disease. *Redox Rep.* **2002**, 7, (4), 199-206.
8. Campesan, S.; Green, E. W.; Breda, C.; Sathyasaikumar, K. V.; Muchowski, P. J.; Schwarcz, R.; Kyriacou, C. P.; Giorgini, F., The Kynurenine Pathway Modulates Neurodegeneration in a *Drosophila* Model of Huntington's Disease. *Curr. Biol.* **2011**, 21, (11), 961-966.
9. Uyttenhove, C.; Pilotte, L.; Théate, I.; Stroobant, V.; Colau, D.; Parmentier, N.; Boon, T.; Van den Eynde, B. J., Evidence for a tumoral immune resistance mechanism based on tryptophan degradation by indoleamine 2,3-dioxygenase. *Nat. Med.* **2003**, 9, (10), 1269-1274.
10. Prendergast, G. C., CANCER Why tumours eat tryptophan. *Nature* **2011**, 478, (7368), 192-194.
11. Triplett, T. A.; Garrison, K. C.; Marshall, N.; Donkor, M.; Blazeck, J.; Lamb, C.; Qerqez, A.; Dekker, J. D.; Tanno, Y.; Lu, W. C.; Karamitros, C. S.; Ford, K.; Tan, B.; Zhang, X. M.; McGovern, K.; Coma, S.; Kumada, Y.; Yamany, M. S.; Sentandreu, E.; Fromm, G.; Tiziani, S.; Schreiber, T. H.; Manfredi, M.; Ehrlich, L. I. R.; Stone, E.; Georgiou, G., Reversal of indoleamine 2,3-dioxygenase-mediated cancer immune suppression by systemic kynurenine depletion with a therapeutic enzyme. *Nat. Biotechnol.* **2018**, 36, (8), 758-764.
12. Li, P.; Xu, W.; Liu, F.; Zhu, H.; Zhang, L.; Ding, Z.; Liang, H.; Song, J., The emerging roles of IDO2 in cancer and its potential as a therapeutic target. *Biomed. Pharmacother.* **2021**, 137, 111295.
13. Pantouris, G.; Serys, M.; Yuasa, H. J.; Ball, H. J.; Mowat, C. G., Human indoleamine 2,3-dioxygenase-2 has substrate specificity and inhibition characteristics distinct from those of indoleamine 2,3-dioxygenase-1. *Amino Acids* **2014**, 46, (9), 2155-63.
14. Efimov, I.; Basran, J.; Sun, X.; Chauhan, N.; Chapman, S. K.; Mowat, C. G.; Raven, E. L., The mechanism of substrate inhibition in human indoleamine 2,3-dioxygenase. *J. Am. Chem. Soc.* **2012**, 134, (6), 3034-41.
15. Jia, J.; Wen, H.; Zhao, S.; Wang, L.; Qiao, H.; Shen, H.; Yu, Z.; Di, B.; Xu, L.; Hu, C., Displacement Induced Off-On Fluorescent Biosensor Targeting IDO1 Activity in Live Cells. *Anal. Chem.* **2019**, 91, (23), 14943-14950.
16. Sono, M., The Roles of Superoxide Anion and Methylene Blue in the Reductive Activation of Indoleamine 2,3-Dioxygenase by Ascorbic Acid or by Xanthine Oxidase-Hypoxanthine. *J. Biol. Chem.* **1989**, 264, (3), 1616-1622.
17. Thomas, S. R.; Terentis, A. C.; Cai, H.; Takikawa, O.; Levina, A.; Lay, P. A.; Freewan, M.; Stocker, R., Post-translational regulation of human indoleamine 2,3-dioxygenase activity by nitric oxide. *J. Biol. Chem.* **2007**, 282, (33), 23778-87.
18. Hirata, F.; Ohnishi, T.; Hayaishi, O., Indoleamine 2,3-dioxygenase. Characterization and properties of enzyme. O2- complex. *J. Biol. Chem.* **1977**, 252, (13), 4637-4642.
19. Yuasa, H. J.; Stocker, R., Methylene blue and ascorbate interfere with the accurate determination of the kinetic properties of IDO2. *FEBS J.* **2021**, 288, (16), 4892-4904.

20. Armstrong, F. A.; Cheng, B.; Herold, R. A.; Megarity, C. F.; Siritanaratkul, B., From Protein Film Electrochemistry to Nanoconfined Enzyme Cascades and the Electrochemical Leaf. *Chem. Rev.* **2023**, 123, (9), 5421-5458.
21. Browne, L. B. F.; Sudmeier, T.; Landis, M. A.; Allen, C. S.; Vincent, K. A., Controlled Biocatalytic Synthesis of a Metal Nanoparticle-Enzyme Hybrid: Demonstration for Catalytic H_2-driven NADH Recycling. *Angew. Chem.-Int. Edit.* **2024**, 63, (27), 6.
22. Adachi, T.; Kitazumi, Y.; Shirai, O.; Kano, K., Direct Electron Transfer-Type Bioelectrocatalysis of Redox Enzymes at Nanostructured Electrodes. *Catalysts* **2020**, 10, (2).
23. Ayikpoe, R.; Ngendahimana, T.; Langton, M.; Bonitatibus, S.; Walker, L. M.; Eaton, S. S.; Eaton, G. R.; Pandelia, M. E.; Elliott, S. J.; Latham, J. A., Spectroscopic and Electrochemical Characterization of the Mycofactocin Biosynthetic Protein, MftC, Provides Insight into Its Redox Flipping Mechanism. *Biochemistry* **2019**, 58, (7), 940-950.
24. Jenner, L. P.; Butt, J. N., Electrochemistry of surface-confined enzymes: Inspiration, insight and opportunity for sustainable biotechnology. *Curr. Opin. Electrochem.* **2018**, 8, 81-88.
25. Luong, J. H. T.; Glennon, J. D.; Gedanken, A.; Vashist, S. K., Achievement and assessment of direct electron transfer of glucose oxidase in electrochemical biosensing using carbon nanotubes, graphene, and their nanocomposites. *Microchim. Acta* **2017**, 184, (2), 369-388.
26. Bhattarai, J. K.; Neupane, D.; Nepal, B.; Mikhaylov, V.; Demchenko, A. V.; Stine, K. J., Preparation, Modification, Characterization, and Biosensing Application of Nanoporous Gold Using Electrochemical Techniques. *Nanomaterials* **2018**, 8, (3).
27. Qiu, H. J.; Xu, H. T.; Liu, L.; Wang, Y., Correlation of the structure and applications of dealloyed nanoporous metals in catalysis and energy conversion/storage. *Nanoscale* **2015**, 7, (2), 386-400.
28. Mie, Y.; Takayama, H.; Hirano, Y., Facile control of surface crystallographic orientation of anodized nanoporous gold catalyst and its application for highly efficient hydrogen evolution reaction. *J. Catal.* **2020**, 389, 476-482.
29. Mie, Y.; Ikegami, M.; Komatsu, Y., Nanoporous Structure of Gold Electrode Fabricated by Anodization and Its Efficacy for Direct Electrochemistry of Human Cytochrome P450. *Chem. Lett.* **2016**, 45, (6), 640-642.
30. Mie, Y.; Takahashi, K.; Itoga, Y.; Sueyoshi, K.; Tsujino, H.; Yamashita, T.; Uno, T., Nanoporous gold based electrodes for electrochemical studies of human neuroglobin. *Electrochem. Commun.* **2020**, 110.
31. Mie, Y.; Takahashi, K.; Torii, R.; Jingkai, S.; Tanaka, T.; Sueyoshi, K.; Tsujino, H.; Yamashita, T., Redox State Control of Human Cytoglobin by Direct Electrochemical Method to Investigate Its Function in Molecular Basis. *Chem. Pharm. Bull.* **2020**, 68, (8), 806-809.
32. Chauhan, N.; Basran, J.; Efimov, I.; Svistunenko, D. A.; Seward, H. E.; Moody, P. C. E.; Raven, E. L., The role of serine 167 in human indoleamine 2,3-dioxygenase: A comparison with tryptophan 2,3-dioxygenase. *Biochemistry* **2008**, 47, (16), 4761-4769.
33. Onuoha, A. C.; Rusling, J. F., ELECTROACTIVE MYOGLOBIN-SURFACTANT FILMS IN A BICONTINUOUS MICROEMULSION. *Langmuir* **1995**, 11, (9), 3296-3301.
34. Sugimoto, Y.; Takeuchi, R.; Kitazumi, Y.; Shirai, O.; Kano, K., Significance of Mesoporous Electrodes for Noncatalytic Faradaic Process of Randomly Oriented Redox Proteins. *J. Phy.l Chem. C* **2016**, 120, (46), 26270-26277.
35. Wang, Q. L.; Lu, G. X.; Yang, B. J., Myoglobin/sol-gel film modified electrode: Direct electrochemistry and electrochemical catalysis. *Langmuir* **2004**, 20, (4), 1342-1347.
36. Chen, S.-M.; Tseng, C.-C., Comparison of the direct electrochemistry of myoglobin and hemoglobin films and their bioelectrocatalytic properties. *J. Electroanal. Chem.* **2005**, 575, (1), 147-160.
37. Yang, W.; Li, Y.; Bai, Y.; Sun, C., Hydrogen peroxide biosensor based on myoglobin/colloidal gold nanoparticles immobilized on glassy carbon electrode by a Nafion film. *Sens. Actuat. B: Chem.* **2006**, 115, (1), 42-48.
38. Kolawole, A. O.; Hixon, B. P.; Dameron, L. S.; Chrisman, I. M.; Smirnov, V. V., Catalytic activity of human indoleamine 2,3-dioxygenase (hIDO1) at low oxygen. *Arch. Biochem. Biophys.* **2015**, 570, 47-57.

 doi:10.20944/preprints202502.0100.v1

39. Zhai, L.; Ladomersky, E.; Bell, A.; Dussold, C.; Cardoza, K.; Qian, J.; Lauing, K. L.; Wainwright, D. A., Quantification of IDO1 enzyme activity in normal and malignant tissues. *Methods Enzymol.* **2019**, 629, 235-256.
40. Liu, X.; Shin, N.; Koblish, H. K.; Yang, G.; Wang, Q.; Wang, K.; Leffet, L.; Hansbury, M. J.; Thomas, B.; Rupar, M.; Waeltz, P.; Bowman, K. J.; Polam, P.; Sparks, R. B.; Yue, E. W.; Li, Y.; Wynn, R.; Fridman, J. S.; Burn, T. C.; Combs, A. P.; Newton, R. C.; Scherle, P. A., Selective inhibition of IDO1 effectively regulates mediators of antitumor immunity. *Blood* **2010**, 115, (17), 3520-30.
41. Pearson, J. T.; Siu, S.; Meininger, D. P.; Wienkers, L. C.; Rock, D. A., In vitro modulation of cytochrome P450 reductase supported indoleamine 2,3-dioxygenase activity by allosteric effectors cytochrome b(5) and methylene blue. *Biochemistry* **2010**, 49, (12), 2647-56.
42. Yue, E. W.; Douty, B.; Wayland, B.; Bower, M.; Liu, X.; Leffet, L.; Wang, Q.; Bowman, K. J.; Hansbury, M. J.; Liu, C.; Wei, M.; Li, Y.; Wynn, R.; Burn, T. C.; Koblish, H. K.; Fridman, J. S.; Metcalf, B.; Scherle, P. A.; Combs, A. P., Discovery of potent competitive inhibitors of indoleamine 2,3-dioxygenase with in vivo pharmacodynamic activity and efficacy in a mouse melanoma model. *J. Med. Chem.* **2009**, 52, (23), 7364-7.
43. Tsujino, H.; Uno, T.; Yamashita, T.; Katsuda, M.; Takada, K.; Saiki, T.; Maeda, S.; Takagi, A.; Masuda, S.; Kawano, Y.; Meguro, K.; Akai, S., Correlation of indoleamine-2,3-dioxigenase 1 inhibitory activity of 4,6-disubstituted indazole derivatives and their heme binding affinity. *Bioorg. Med. Chem. Lett.* **2019**, 29, (19), 126607.
44. Lukaszewski, M.; Soszko, M.; Czerwinski, A., Electrochemical Methods of Real Surface Area Determination of Noble Metal Electrodes - an Overview. *Int. J. Electrochem. Sci.* **2016**, 11, (6), 4442-4469.
45. Trashin, S.; de Jong, M.; Meynen, V.; Dewilde, S.; De Wael, K., Attaching Redox Proteins onto Electrode Surfaces by using bis-Silane. *ChemElectroChem* **2016**, 3, (7), 1035-1038.
46. Fukunishi, Y.; Mikami, Y.; Kubota, S.; Nakamura, H., Multiple target screening method for robust and accurate in silico ligand screening. *J. Mol. Graph.* **2006**, 25, (1), 61-70.
47. Fukunishi, Y.; Mikami, Y.; Takedomi, K.; Yamanouchi, M.; Shima, H.; Nakamura, H., Classification of chemical compounds by protein-compound docking for use in designing a focused library. *J. Med. Chem.* **2006**, 49, (2), 523-533.
48. Trott, O.; Olson, A. J., Software News and Update AutoDock Vina: Improving the Speed and Accuracy of Docking with a New Scoring Function, Efficient Optimization, and Multithreading. *J. Comput. Chem.* **2010**, 31, (2), 455-461.
49. Morris, G. M.; Huey, R.; Lindstrom, W.; Sanner, M. F.; Belew, R. K.; Goodsell, D. S.; Olson, A. J., AutoDock4 and AutoDockTools4: Automated Docking with Selective Receptor Flexibility. *J. Comput. Chem.* **2009**, 30, (16), 2785-2791.